

Tuning the Case-Dependent Parameters of Relaxation Zones for Flow Simulations With Strongly Reflecting Bodies in Free-Surface Waves

Robinson Perić^{a,1}, Vuko Vukčević^b, Moustafa Abdel-Maksoud^a, Hrvoje Jasak^{b,c}

^a*Hamburg University of Technology (TUHH), Institute for Fluid Dynamics and Ship Theory (M8), Hamburg, Germany*

^b*University of Zagreb, Faculty of Mechanical Engineering and Naval Architecture, Ivana Lučića 5, Zagreb, Croatia*

^c*Wikki Ltd, 459 Southbank House, SE1 7SJ, London, United Kingdom*

Abstract

In finite-volume-based flow simulations with free-surface waves, wave reflections at the domain boundaries must be minimized. This can be achieved by introducing source terms in the governing equations, for which two different approaches are widely used, namely ‘forcing zones’ and ‘relaxation zones’. Both approaches have case-dependent parameters, which must be tuned to the waves to obtain reliable results. For forcing zones, a theory to predict reflection coefficients was proposed by Perić and Abdel-Maksoud (2018); its use for tuning forcing zone parameters was demonstrated via comparison to flow simulation results for regular, long-crested waves in deep-water.

This paper extends their theory to apply to relaxation zones, which blend two solutions by fading from one to the other. The theory predictions are validated via flow simulations using two different codes, Siemens STAR-CCM+ and the `foam-extend` Naval Hydro Pack. The validation is performed via parameter studies for different blending functions, zone thicknesses and source term magnitudes. Simulations are run for long-crested waves under shallow-water and deep-water conditions in 2D and for deep-water conditions in 3D with an additional strongly reflecting body within the domain. The results

¹Corresponding author. Tel. +49 40 42878 6031.
E-mail adress: robinson.peric@tuhh.de

show that the theory satisfactorily predicts the optimum relaxation zone parameters. Recommendations for engineering practice are provided, so that with this work theory predictions should be available for all open and commercial finite-volume-based flow solvers.

Keywords: Relaxation zones, free-surface waves, reflection coefficient, case-dependent parameters, theory prediction

1. Introduction

In finite-volume-based flow simulations with free-surface waves, undesired wave reflections at the boundaries of the computational domain must be minimized. This can be achieved by introducing source terms in the governing equations, for which two different approaches are widely used, namely ‘forcing zones’ and ‘relaxation zones’. *Forcing zones*, also called absorbing layers, sponge layers, damping zones, explicit Euler method, etc. (Choi and Yoon, 2009; Kim et al., 2012; Park et al., 1999; Park et al., 2001; Perić and Abdel-Maksoud, 2016; Schmitt and Elsaesser, 2015; Wöckner-Kluwe, 2013), apply source terms in one or more governing equations to force the solution towards a reference solution as described in Sect. 2. In contrast, *relaxation zones* (Chen et al., 2006; Jacobsen et al., 2012; Mayer et al., 1998; Meyer et al., 2017; Schmitt and Elsaesser, 2015; Vukčević et al., 2016a and 2016b) blend the solution of all governing equations towards a reference solution as described in Sect. 3.

Both approaches have case-dependent parameters, which must be tuned to the waves to obtain reliable results. Although it was found that these parameters must be adjusted for every simulation (Mani, 2012; Perić and Abdel-Maksoud, 2018), it is still common practice that the default coefficients are used or that the coefficients are selected according to “trial and error” (Colonus, 2004, p. 337), which can lead to significant errors (Perić and Abdel-Maksoud, 2016). This practice was due to a lack of tools for predicting the reflection behavior of these approaches.

Recently, Perić and Abdel-Maksoud (2018) presented an analytical approach to predict reflection coefficients depending on the case-dependent parameters for forcing zones. Their theory was validated against results from 2D flow simulations of long-crested waves. It was found that the optimum parameter settings and the corresponding reflection coefficients of forcing zones were predicted with satisfactory accuracy for practical purposes.

Therefore, the aim of the present work is to extend the theory from Perić and Abdel-Maksoud (2018) to hold for relaxation zones as well. The corresponding derivation is given in Sect. 4 in a general manner so that it should be easily applicable to all implementations of relaxation zones. A computer code for evaluating the theory is published as free software alongside this work.

Subsequently, Sects. 6 to 7 validate the theory predictions for reflection coefficients via flow simulations using two different solvers, Siemens STAR-CCM+ and the `foam-extend` Naval Hydro Pack. The validation is performed via parameter studies for different blending functions, zone thicknesses, source term magnitudes and reference solutions. Simulations are run for long-crested waves under shallow-water and deep-water conditions in 2D and for deep-water conditions in 3D with an additional strongly reflecting body within the domain. Based on these findings, recommendations for setting up relaxation zones are given.

2. Forcing zones

Forcing zones introduce source terms in one or more of the governing equations for conservation of momentum and volume fraction

$$\frac{d}{dt} \int_V \rho u_i dV + \int_S \rho u_i (\mathbf{v} - \mathbf{v}_g) \cdot \mathbf{n} dS = \int_S (\tau_{ij} \mathbf{i}_j - p \mathbf{i}_i) \cdot \mathbf{n} dS + \int_V \rho \mathbf{g} \cdot \mathbf{i}_i dV + \int_V \rho q_i dV \quad , \quad (1)$$

$$\frac{d}{dt} \int_V \alpha dV + \int_S \alpha (\mathbf{v} - \mathbf{v}_g) \cdot \mathbf{n} dS = \int_V q_\alpha dV \quad , \quad (2)$$

with volume V of control volume (CV) bounded by the closed surface S , fluid velocity $\mathbf{v} = (u_1, u_2, u_3)^T = (u, v, w)^T$, grid velocity \mathbf{v}_g , unit vector \mathbf{n} normal to S and pointing outwards, time t , pressure p , fluid density ρ , components τ_{ij} of the viscous stress tensor, unit vector \mathbf{i}_j in direction x_j , and volume fraction α of water. The results in this work apply regardless which formulation for τ_{ij} is chosen or whether it is neglected altogether, since wave propagation is an approximately inviscid phenomenon.

The source terms for forcing of volume fraction, q_α , and momentum, q_i , are

$$q_i = \gamma b(\tilde{x})(u_{i,\text{ref}} - u_i) \quad , \quad (3)$$

$$q_\alpha = \gamma b(\tilde{x}) (\alpha_{\text{ref}} - \alpha) \quad , \quad (4)$$

with reference velocity component $u_{i,\text{ref}}$, reference volume fraction α_{ref} , forcing strength γ and blending function $b(\tilde{x})$. In this work, exponential and power blending functions will be used

$$b(\tilde{x}) = \left(\frac{e^{((x_d - \tilde{x})/x_d)^n} - 1}{e^1 - 1} \right) \quad , \quad (5)$$

$$b(\tilde{x}) = \left[\cos^2 \left(\frac{\pi}{2} + \frac{\pi}{2} \left(\frac{x_d - \tilde{x}}{x_d} \right) \right) \right]^n \quad , \quad (6)$$

$$b(\tilde{x}) = \left(\frac{x_d - \tilde{x}}{x_d} \right)^n \quad , \quad (7)$$

where \tilde{x} is the shortest distance to the closest domain boundary to which a forcing zone of thickness x_d is attached (confer Fig. 2), and n regulates the shape of the blending function.

Forcing zones have three case-dependent parameters which must be tuned to achieve reliable reduction of undesired wave reflections². These are forcing strength γ , which regulates the magnitude of the source term, blending function $b(\tilde{x})$, which regulates how the magnitude of the source term varies within the forcing zone, and zone thickness x_d . Perić and Abdel-Maksoud (2016) showed that γ and x_d scale as

$$\gamma \propto \omega, \quad x_d \propto \lambda \quad , \quad (8)$$

so in this manner their settings from one successful simulation can be applied to another simulation for a different wave.

Recently Perić and Abdel-Maksoud (2018) presented a theory for predicting the reflection coefficients for forcing zones and published a simple computer program to evaluate the theory as free software, which can be downloaded from <https://github.com/wave-absorbing-layers/absorbing-layer-for-free-surface-waves>. The theory predictions were validated against results from flow simulations with long-crested waves in

²Perić and Abdel-Maksoud (2016, 2018) showed that, for practical discretizations, the behavior of the forcing zone can be considered discretization-independent, i.e. independent of time step size, mesh size, and the choice and order of the discretization schemes.

deep water. Simulations were run for a wide range of values for γ , x_d , and $b(\tilde{x})$ and theory predictions turned out to be of satisfactory accuracy for practical purposes. Thus using this theory is currently the recommended way of tuning the case-dependent forcing zone parameters.

3. Relaxation zones

Relaxation zones blend, say a general transport equation \mathcal{T} for transport quantity ϕ , over to a reference solution via

$$(1 - b(\tilde{x})) \mathcal{T} + \frac{b(\tilde{x})}{\tau} \mathcal{R} = 0 \quad , \quad (9)$$

where $b(\tilde{x})$ is a blending function such as e.g. Eqs. (5) to (7), \mathcal{T} corresponds e.g. to Eqs. (1) and (2), and \mathcal{R} corresponds to $\int_V (\phi - \phi_{\text{ref}}) dV$ with reference solution ϕ_{ref} for transport quantity ϕ . The relaxation parameter τ has unit [s] and regulates the magnitude of the source term in such a way that a large value of τ implicates a small source term and vice versa.

In contrast to forcing zones, which in literature are also frequently applied to just a single governing equation, relaxation zones usually blend all governing equations except for the pressure-correction equation. Another difference between forcing zones and relaxation zones is that relaxation zones ‘blend out’ all terms except the source terms in the governing equations via the factor $(1 - b(\tilde{x}))$; forcing zones do not have this factor, thus with forcing zones the whole governing equations remain active in the whole domain, whereas within relaxation zones as in Eqs. (10) and (11), the terms from the governing equations that are active in the solution domain of interest are faded out and the reference solution is faded in.

Hence the conservation equations for momentum and volume fraction take the form

$$\begin{aligned} (1 - b(\tilde{x})) & \left[\frac{d}{dt} \int_V \rho u_i dV + \int_S \rho u_i (\mathbf{v} - \mathbf{v}_g) \cdot \mathbf{n} dS \right. \\ & \left. - \int_S (\tau_{ij} \mathbf{i}_j - p \mathbf{i}_i) \cdot \mathbf{n} dS - \int_V \rho \mathbf{g} \cdot \mathbf{i}_i dV \right] \\ & + \frac{b(\tilde{x})}{\tau} \left[\int_V \rho (u_i - u_{i,\text{ref}}) dV \right] = 0 \quad , \quad (10) \end{aligned}$$

$$(1 - b(\tilde{x})) \left[\frac{d}{dt} \int_V \alpha \, dV + \int_S \alpha (\mathbf{v} - \mathbf{v}_g) \cdot \mathbf{n} \, dS \right] + \frac{b(\tilde{x})}{\tau} \left[\int_V (\alpha_i - \alpha_{i,\text{ref}}) \, dV \right] = 0 \quad (11)$$

with reference velocities $u_{i,\text{ref}}$ and reference volume fraction $\alpha_{i,\text{ref}}$.

In this work, the relaxation is implemented implicitly as described in Jasak et al. (2015) and Vukčević et al. (2016a, 2016b). Note that also explicit implementations as in Jacobsen et al. (2012) are possible.

As with forcing zones, also relaxation zones have three case-dependent parameters, i.e. relaxation parameter τ , blending function $b(\tilde{x})$, and relaxation zone thickness x_d .

4. Theory for predicting reflection coefficients for relaxation zones

In this section, the theory from Perić and Abdel-Maksoud (2018) is extended to predict the reflection-reducing behavior of relaxation zones. As a brief review, the theory from Perić and Abdel-Maksoud (2018) was derived for the case of long-crested waves with a forcing zone via Eq. (3) for the horizontal momentum to minimize undesired wave reflections as sketched in Fig. 2. It can be shown that this problem is equivalent to solving the wave equation for the stream function with an additional forcing term

$$\psi_{tt} = c^2 \psi_{xx} + \gamma b(x) (\psi_{t,\text{ref}} - \psi_t) \quad , \quad (12)$$

with temporal derivative of the reference stream function $\psi_{t,\text{ref}}$. Then, the continuous blending function is ‘discretized’, i.e. replaced by a piece-wise constant blending function as illustrated in Fig. 1. Thus the wave number per piece-wise constant segment of $b(x)$ is

$$k_j = \sqrt{\frac{\omega^2 + i\omega\gamma b(\sum_{n=1}^{j-1} x_{d_n} + \frac{1}{2}x_{d_j})}{c^2}} \quad , \quad (13)$$

with angular wave frequency ω , forcing strength γ , phase velocity c , and thickness $x_{d,j}$ of segment j .

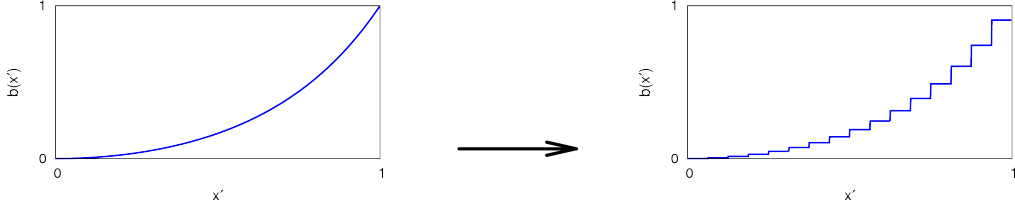


Figure 1: Replace continuous by piece-wise constant blending function $b(x')$

The benefit of this approach is that then the theory holds for every possible blending function. Since the approach is somewhat analogous to the way in which the source terms are applied in the flow simulations, also the influence of the discretization can be considered. With increasing resolution, the theoretical results were found to converge to the solution of the continuous problem.

By requiring that velocities and displacements must be continuous everywhere, the solution to Eq. (12) for every segment j is

$$\psi_j = \psi_0 \left(\prod_{n=0}^{j-1} C_{T_n} \right) \cdot \left[e^{i(\sum_{n=1}^{j-1} k_n x_{d_n} + k_j (x - \sum_{n=1}^{j-1} x_{d_n}))} - C_{R_j} e^{i(\sum_{n=1}^{j-1} k_n x_{d_n} + k_j 2x_{d_j} - k_j (x - \sum_{n=1}^{j-1} x_{d_n}))} \right], \quad (14)$$

$$\psi_0 = \frac{H\omega \sinh(k_0(z+h))}{2k_0 \sinh(k_0 h)} e^{i(-\omega t)}, \quad (15)$$

with wave height H , angular wave frequency ω , wave number k_j , vertical coordinate z , time t , local transmission coefficient C_{T_j} , and local reflection coefficient C_{R_j} . Set the inlet boundary ($x = 0$) as perfectly transparent, i.e. $C_{T_0} = 1$ and $C_{R_0} = 0$, and the opposite boundary ($x = L_x$) as perfectly reflecting, i.e. $C_{T_{j_{\max}}} = 0$ and $C_{R_{j_{\max}}} = 1$, then one obtains

$$C_{T_j} = \frac{1 - C_{R_j}}{1 - C_{R_{j+1}} e^{i(k_{j+1} 2x_{d_{j+1}})}} , \quad (16)$$

$$\beta_{j+1} = \frac{1 + C_{R_{j+1}} e^{i(k_{j+1} 2x_{d_{j+1}})}}{1 - C_{R_{j+1}} e^{i(k_{j+1} 2x_{d_{j+1}})}} , \quad (17)$$

$$C_{R_j} = \frac{k_{j+1}\beta_{j+1} - k_j}{k_{j+1}\beta_{j+1} + k_j} \quad , \quad (18)$$

If the forcing zone starts at segment 1, the global reflection coefficient is

$$C_R = |C_{R_1}| = \sqrt{\text{Re}\{C_{R_1}\}^2 + \text{Im}\{C_{R_1}\}^2} \quad . \quad (19)$$

where $\text{Re}\{X\}$ and $\text{Im}\{X\}$ denote the real and the imaginary part of the complex number X . Assuming that a forcing in one governing equation acts immediately on all other governing equations, then the above solution equals the solution for applying forcing with $\gamma/4$ in all four governing equations, i.e. in Eqs. (1) to (4). It was found that this last assumption is not entirely fulfilled if the forcing is (also) applied to transverse (i.e. horizontal) momentum and if additionally large changes in source term magnitude occur over a short part of the forcing zone; then simulation results for reflection coefficients were lower than theory predictions. This occurred e.g. when forcing strength γ was chosen to be larger than optimum, so that the waves are mainly reflected close to the entrance of the forcing zone, whereas for optimum forcing strength reflections occur more evenly throughout the whole forcing zone. The latter is beneficial since destructive interference of partial wave reflections occurring everywhere within the forcing zone was found to be a key mechanism in how forcing zones reduce undesired wave reflections.

The behavior of the forcing zone was found to be different, depending on which governing equations a forcing is applied to: For forcing of horizontal momentum, the theory predicted the flow inside the forcing zone with high accuracy. For forcing in all governing equations, the theory rather gave an upper bound for the reflection coefficient. For further details concerning the above derivation and discussion, the reader is referred to Perić and Abdel-Maksoud (2018).

To extend this theory to relaxation zones, multiply Eqs. (10) and (11) by the factor $1/(1 - b(\tilde{x}))$. Then the relaxation can be interpreted as a forcing, where the source terms in Eqs. (1) and (2) are

$$q_i = \frac{b(\tilde{x})}{\tau(1 - b(\tilde{x}))} (u_{i,\text{ref}} - u_i) \quad , \quad (20)$$

$$q_\alpha = \frac{b(\tilde{x})}{\tau(1 - b(\tilde{x}))} (\alpha_{i,\text{ref}} - \alpha_i) \quad , \quad (21)$$

with blending function $b(\tilde{x})$, relaxation parameter τ , velocity u_i , reference velocity $u_{i,\text{ref}}$, volume fraction α_i , and reference volume fraction $\alpha_{i,\text{ref}}$. Thus by setting γ in Eqs. (12) and (19) to

$$\gamma = \frac{1}{\tau(1 - b(\tilde{x}))} \quad , \quad (22)$$

the theory is extended to relaxation zones. Note that Eqs. (20) to (22) do not become singular, since for the piecewise-constant blending in Eq. (13) $b(\tilde{x})$ is evaluated at the center of each segment and thus is always < 1 .

A simple computer program to evaluate the theory for predicting the relaxation zone behavior has been published as free software. The source code and manual can be downloaded from the following link: <https://github.com/wave-absorbing-layers/relaxation-zones-for-free-surface-waves>.

5. Simulation setup

For the 2D-simulations in Sect. 6, the solution domain is box-shaped as seen in Fig. 2. The origin of the coordinate system lies at the calm free-surface level, with z pointing upwards and x pointing in wave propagation direction. The domain dimensions are $0 \text{ m} \leq x \leq 24 \text{ m}$, $-2 \text{ m} \leq z \leq 0.24 \text{ m}$ for the simulations with deep water conditions (water depth $h \approx 0.5\lambda$) and $0 \text{ m} \leq x \leq 24 \text{ m}$, $-0.2 \text{ m} \leq z \leq 0.01 \text{ m}$ for the simulations with shallow water conditions ($h \approx 0.05\lambda$). The simulations are run as quasi-2D, i.e. with only one layer of cells in y -direction and the y -normal boundaries set to symmetry planes. Waves are generated by prescribing volume fraction and velocities according to Rienecker and Fenton's (1981) stream function wave theory (64th order) at the velocity inlet $x = 0$. The deep-water cases had wave period $T = 1.6 \text{ s}$, wavelength $\lambda \approx 4 \text{ m}$ and wave height $H = 0.16 \text{ m}$. The shallow-water cases had wave period $T = 2.893 \text{ s}$, wavelength $\lambda \approx 4 \text{ m}$ and wave height $H = 0.009 \text{ m}$. The waves travel in positive x -direction towards a relaxation zone attached to the pressure outlet boundary at $x = 24 \text{ m}$. At the outlet, pressure and volume fraction are prescribed according to the calm free-surface solution. In the relaxation zone, the waves are blended towards a reference solution via Eqs. (10) to (11) to reduce undesired wave reflections. Simulations were run for different values of zone thickness x_a , different blending functions $b(\tilde{x})$, and different reference solutions. The bottom boundary

had a slip-wall boundary condition and at the top boundary atmospheric pressure was prescribed.

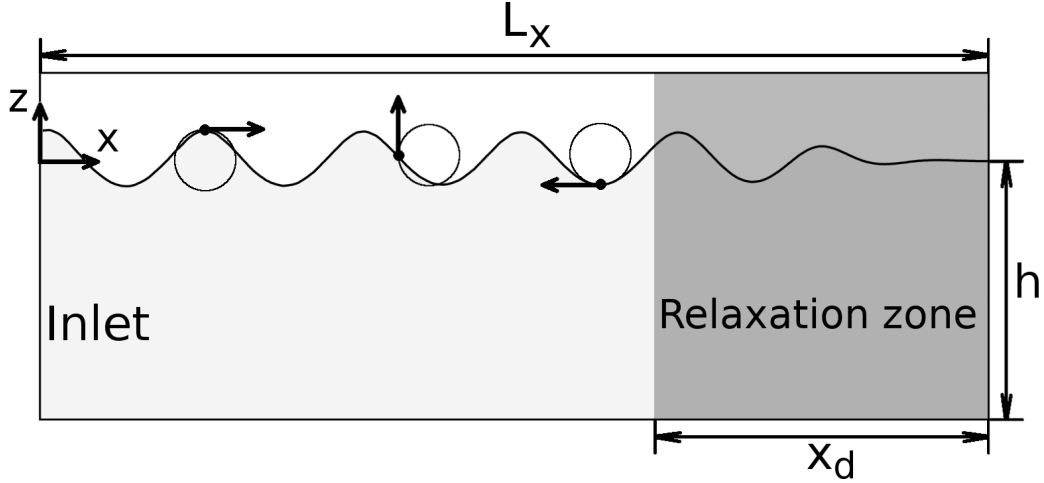


Figure 2: Solution domain filled with air (white) and water (light gray, water depth h), velocity inlet at $x = 0$ and relaxation zone (shaded dark gray) with thickness x_d ; three fluid particles (black dots) are sketched with their particle paths (circles) and velocity vectors (arrows)

The simulations in this work were run using the open-source solver `foam-extend` version 4.1, a community driven fork of the solver OpenFOAM (Weller et al., 1998), combined with the commercial software Naval Hydro Pack. The governing equations are Eqs. (10) to (11), so no turbulence modeling was used. All approximations were of second order. The solvers were conjugate gradient with Cholesky preconditioner for pressures, bi-conjugate gradient with ILU0 preconditioner for volume fraction and velocities and the PIMPLE scheme was used with two pressure correction steps per each of the two nonlinear iterations in a given time-step, and two iterations per time step for pressure correction. No under-relaxation was used. In all simulations, the Courant number $C = |\mathbf{u}|\Delta t/\Delta x$ was well below 0.4. Further information on the discretization of and solvers for the governing equations can be found in Ferziger and Perić (2002) and the flow solver manuals.

In Sect. 6.3, selected simulations were rerun with the commercial flow solver STAR-CCM+ version 10.6 by Siemens (formerly CD-adapco), using the grid and simulation setup from Perić and Abdel-Maksoud (2018), except

that the forcing zones in STAR-CCM+ were tuned via Eqs. (20) to (22) in such a way that they mimic the behavior of the relaxation zones from the Naval Hydro Pack.

Figure 3 shows the rectilinear grid with local mesh refinement. The free surface stays at all time within the zone with the finest mesh, with 25 (coarse grid), 35 (medium grid), or 50 (fine grid) cells per wavelength λ , and 5 (coarse grid), 7 (medium grid), or 10 (fine grid) cells per wave height H . The grid consists of 12 000 (coarse grid), 17 000 (medium grid), or 48 000 (fine grid) cells. The time-step was $0.01 \text{ s} = T/160$ (coarse grid), $0.0071 \text{ s} = T/226$ (medium grid), or $0.005 \text{ s} = T/320$ (fine grid).

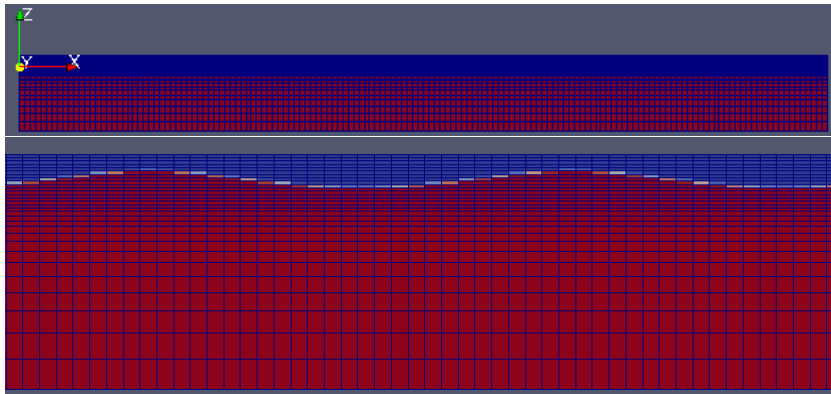


Figure 3: Mesh for 2D simulations with coarse mesh; far view (top) and close-up (bottom); the color denotes the volume fraction (red: water, blue: air)

For the 3D-simulations in Sect. 7, the setup is identical to the deep-water 2D simulations, with the following exceptions. The domain has dimensions $0 \text{ m} \leq x \leq 10 \text{ m}$, $0 \text{ m} \leq y \leq 10 \text{ m}$, $-5 \text{ m} \leq z \leq 5 \text{ m}$, so the water depth is $h = 5 \text{ m}$ as seen in Fig. 4. In the center of the domain, a semi-submerged pontoon with dimensions $1 \text{ m} \times 1 \text{ m} \times 1 \text{ m}$ is held in fixed position. It has a draft of $D = 0.5 \text{ m}$ and slip wall boundary conditions. The wave has period $T = 1.6 \text{ s}$, wave height $H = 0.4 \text{ m}$, wavelength $\lambda \approx 4.3 \text{ m}$ and steepness $H/\lambda \approx 71\%$ of the breaking steepness.

The free surface is discretized by 12.9 (coarse grid), 25.8 (medium grid), or 38.7 (fine grid) cells per wavelength λ and 2 (coarse), 4 (medium), or 6 cells per wave height H as shown in Fig. 4. Per wave period 160 (coarse grid), 225 (medium grid), or 320 (fine grid) time steps were used.

The relaxation zone thickness was $x_d = 3 \text{ m} \approx 0.7\lambda$ and power blending according to Eq. (7) with exponent $n = 0.46$ was used. Simulations are run for different relaxation parameters $0.001 \text{ s} \leq \tau \leq 1000 \text{ s}$. This setup was expected to be close to the minimum domain size for the simulation of such a strongly reflecting body.

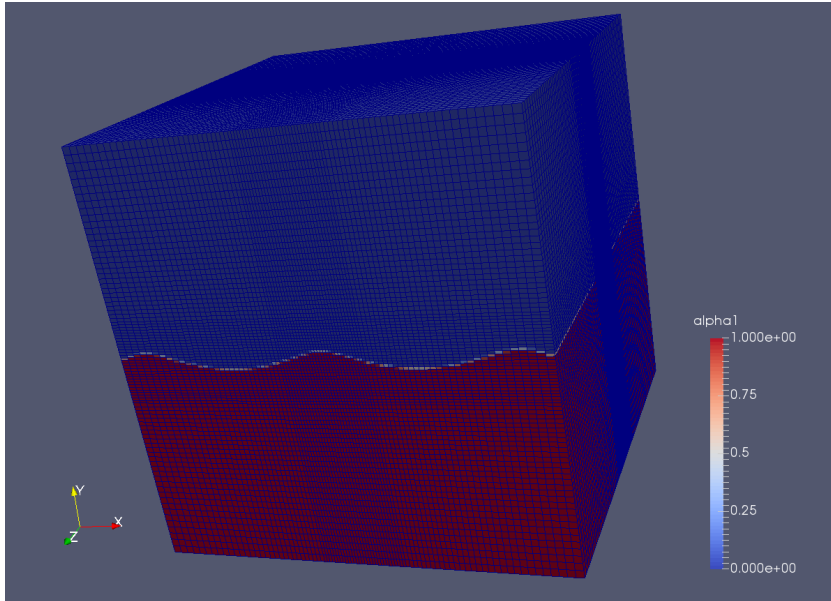


Figure 4: Fine mesh for 3D simulations with initialized volume fraction

6. Results of 2D-flow simulations

This section validates the theory predictions via 2D flow simulations. The reflection coefficient C_R is calculated as in Ursell et al. (1960) as

$$C_R = (H_{\max} - H_{\min}) / (H_{\max} + H_{\min}) \quad , \quad (23)$$

where H_{\max} is the maximum and H_{\min} the minimum value of the wave height envelope, measured over a distance in wave propagation direction of 1.25λ next to the relaxation zone. It holds $0 \leq C_R \leq 1$, with $C_R = 1$ for perfect wave reflection and $C_R = 0$ for no wave reflection. This approach was found to be reasonably accurate in Perić and Abdel-Maksoud (2018) for the investigated moderate wave steepnesses, where it had a comparatively low

background noise, so that reflection coefficients down to roughly 1 – 2% can be detected.

6.1. Discretization dependence study for using relaxation zones to damp waves

First, the relaxation zone is set up to damp the waves by setting the hydrostatic solution for the calm free surface as reference solution in Eqs. (10) to (11). Exponential blending with coefficient $n = 3.5$ is used, which is the default setting in the Naval Hydro Pack. Simulations are run for different values of zone thickness x_d and relaxation parameter τ .

Figure 5 shows that the theory predicts the optimum parameter settings reasonably well, and the theoretical reflection coefficients C_R can be taken as an upper bound for the recorded values. For this setting, the Naval Hydro Pack default value of τ (i.e. the time step, here $\Delta t = 0.005$ s) is comparatively close to the optimum value of ca. $0.1 \text{ s} \lesssim \tau \lesssim 0.5 \text{ s}$, though not as close as the theory predictions. However, with the default setting $\tau = \Delta t$ the reflection coefficients will increase for finer time steps, since Perić and Abdel-Maksoud (2018) showed that the reflection behavior of relaxation zones can be considered independent of the discretization, which is supported by the results in Fig. 6. For example for a time step of $\Delta t \lesssim 0.001$ s, the same reduction of undesired wave reflections, that would be obtained with default settings for a relaxation zone thickness $x_d = 1\lambda$, can be obtained for a zone thickness of only $x_d = 0.5\lambda$ when τ is tuned according to the theory.

For many engineering applications though, the results suggest that setting $\tau = \Delta t$ when using the default blending function should provide acceptable reduction of undesired wave reflections, if the zone thickness is chosen sufficiently large; for $x_d \geq 1.0\lambda$, reflection coefficients of $C_R < 10\%$ can be expected. Since $\Delta t \propto T$, the default value for τ in the Naval Hydro Pack also scales correctly (confer Eq. (8)), so that the default coefficients provide acceptable 'black box' default settings.

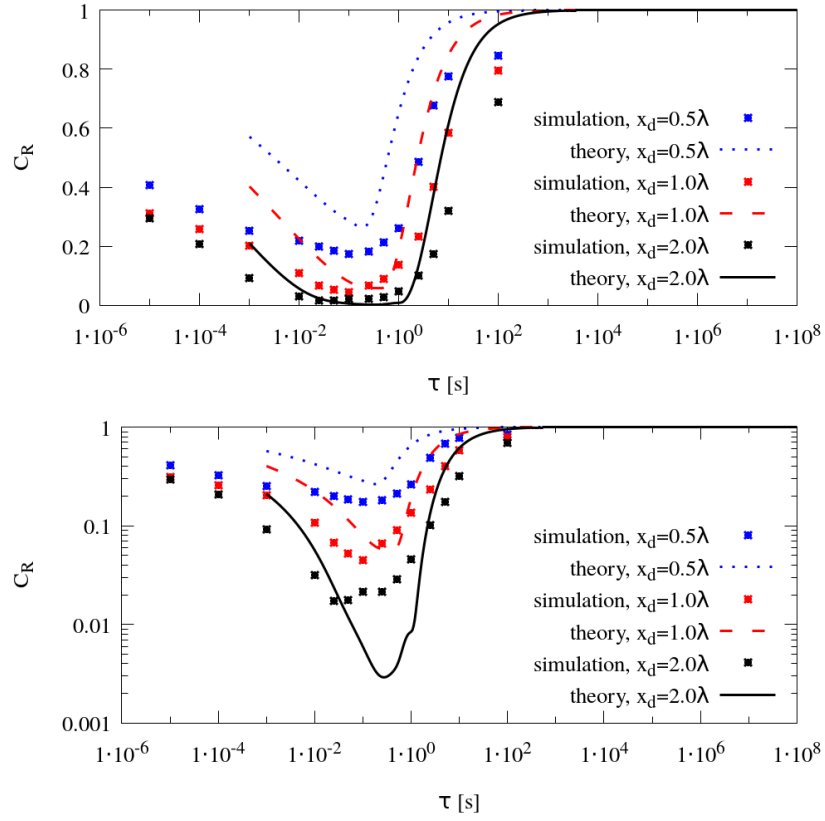


Figure 5: Theory predictions and simulation results for reflection coefficient C_R over relaxation parameter τ , for deep-water waves with period $T = 1.6$ s; for different relaxation zone thickness x_d , exponential blending via Eq. (5) with exponent $n = 3.5$ and coarse discretization

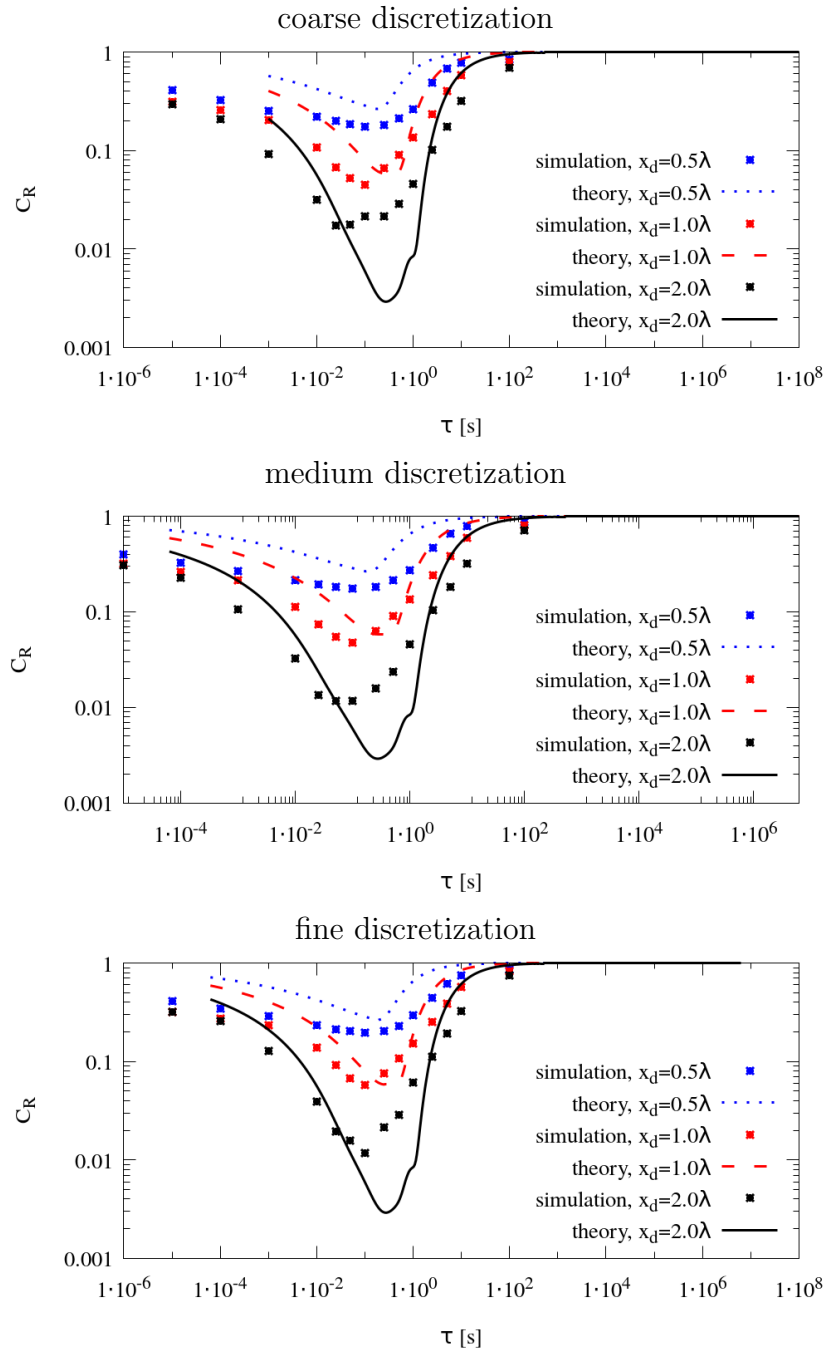


Figure 6: As Fig. 5, except for coarse, medium, and fine discretization; as theory suggests, results can be considered discretization-independent for practical discretizations

6.2. Using relaxation zones to damp waves in shallow water

The theory in Sect. 4 was derived to hold for all water depths and Fig. 7 confirms that the predictions are of satisfactory accuracy also for shallow water depths. Compared to the deep-water case, the simulation results for the reflection coefficients are lower for smaller-than-optimum values of relaxation parameter τ , but show no substantial qualitative difference otherwise.

Recently, Carmigniani and Violeau (2018) used forcing zones for horizontal and vertical velocities to damp regular waves in finite-difference simulations for linearized Navier-Stokes-equations; they observed a decrease in the optimum value of the source term strength for decreasing water depth. In contrast, the present results show no significant dependence of the water depth on the optimum value of relaxation parameter τ .

However, one should point out that in Figs. 5 to 11 the optimum τ from the simulation results is sometimes slightly larger or smaller than theory predicts. Since there does not seem to be a clear trend in these deviations and since they are comparatively small, this detail seems to be of minor importance for engineering practice.

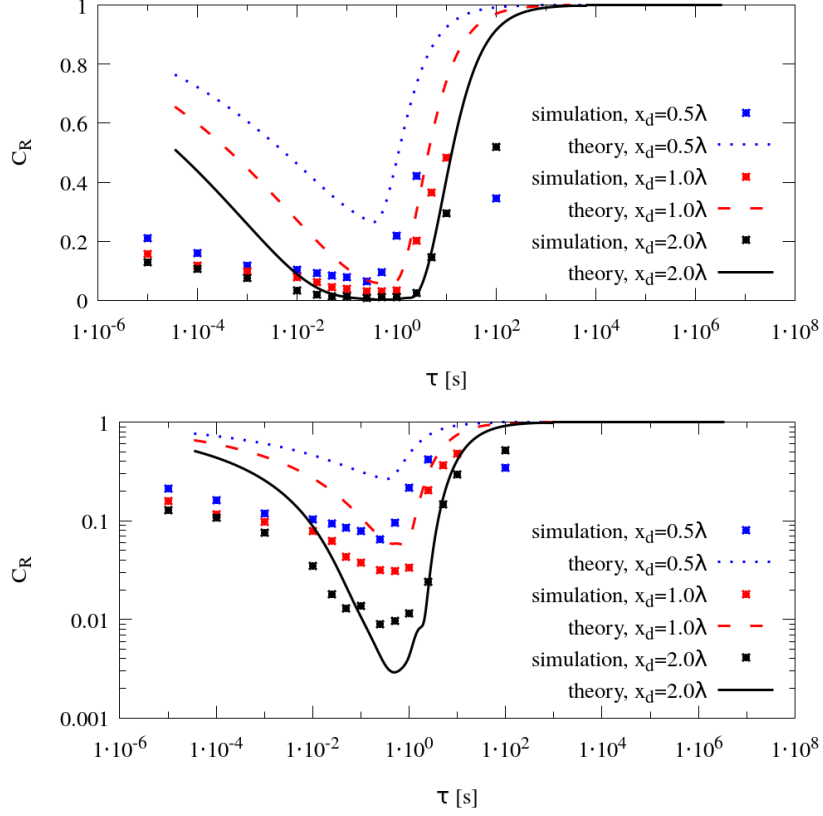


Figure 7: As Fig. 5, except for shallow water waves with period $T = 2.893$ s

6.3. Comparison to relaxation zone in a different CFD code

Similar to the way in which Sect. 4 extended the theory for forcing zones to relaxation zones, the behavior of relaxation zones can be 'modeled' using forcing zones. To demonstrate this, simulations for the wave from Sect. 6.1 are rerun with a different flow solver, STAR-CCM+ by Siemens. STAR-CCM+ does not have relaxation zones implemented, but forcing zones according to Eqs. (1) and (2) are available.

To obtain relaxation-zone-like behavior, Eqs. (20) and (21) are introduced as source terms in Eqs. (1) and (2). This formulation has the disadvantage that at the domain boundary $b(\tilde{x}) = 1$ so that $q_i, q_\alpha \rightarrow \infty$. Thus stability problems must be expected when $\tau \rightarrow 0$ and when the cell sizes close to the domain boundary are small. The STAR-CCM+ simulations indeed blew

up for small τ values, which is the reason for the missing data points ($\tau \leq 10^{-2}$ s) in Figs. 8 and 9. These stability issues are due to the different implementation of forcing zones and relaxation zones, so using one approach to ‘mimic’ the other would theoretically give the same results, but practically can be significantly less stable for certain settings by allowing source terms to become extremely large.

Note that no stability issues occur when using forcing zones (Eqs. (1) to (4)) or relaxation zones (Eqs. (10) and (11)) in the way they were intended, as the present results and findings in Perić and Abdel-Maksoud (2018) demonstrate. Further, comparing the present results to the ones from Perić and Abdel-Maksoud (2018) indicates that forcing zones and relaxation zones both work equally satisfactory when correctly set up.

Figures 8 and 9 show that the results of the two different codes agree well. Thus one can confidently expect both the present results and the theory from Sect. 4 to be applicable to all CFD solvers using any implementation of relaxation zones.

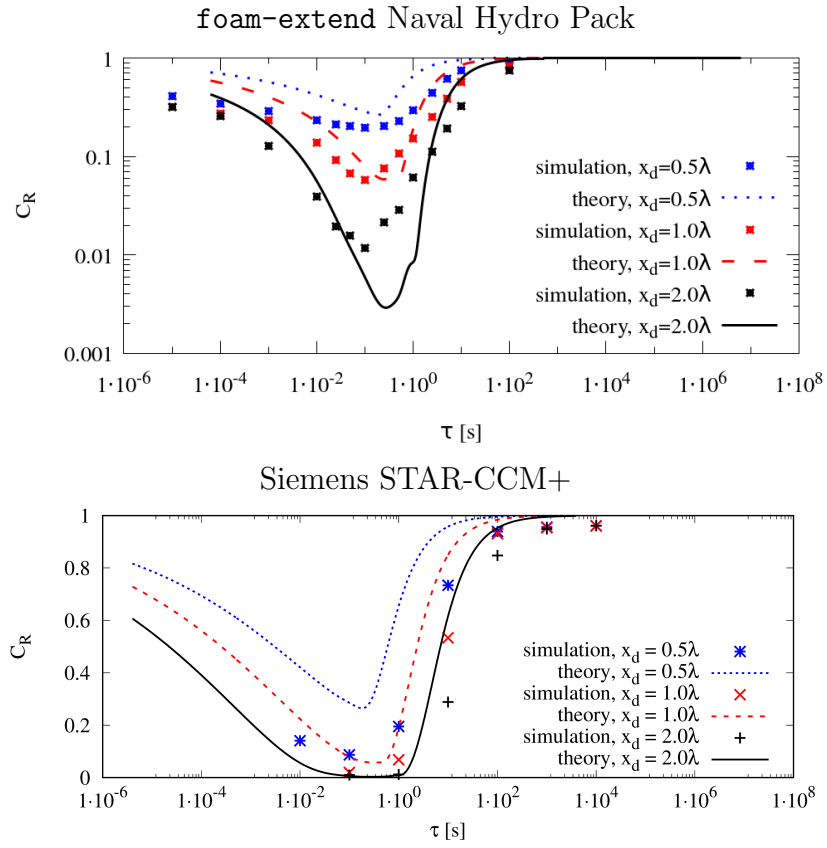


Figure 8: Theory predictions and simulation results from two different CFD codes for reflection coefficient C_R over relaxation parameter τ , for deep-water waves with period $T = 1.6$ s; for different relaxation zone thickness x_d , exponential blending via Eq. (5) with exponent $n = 3.5$, and fine discretization

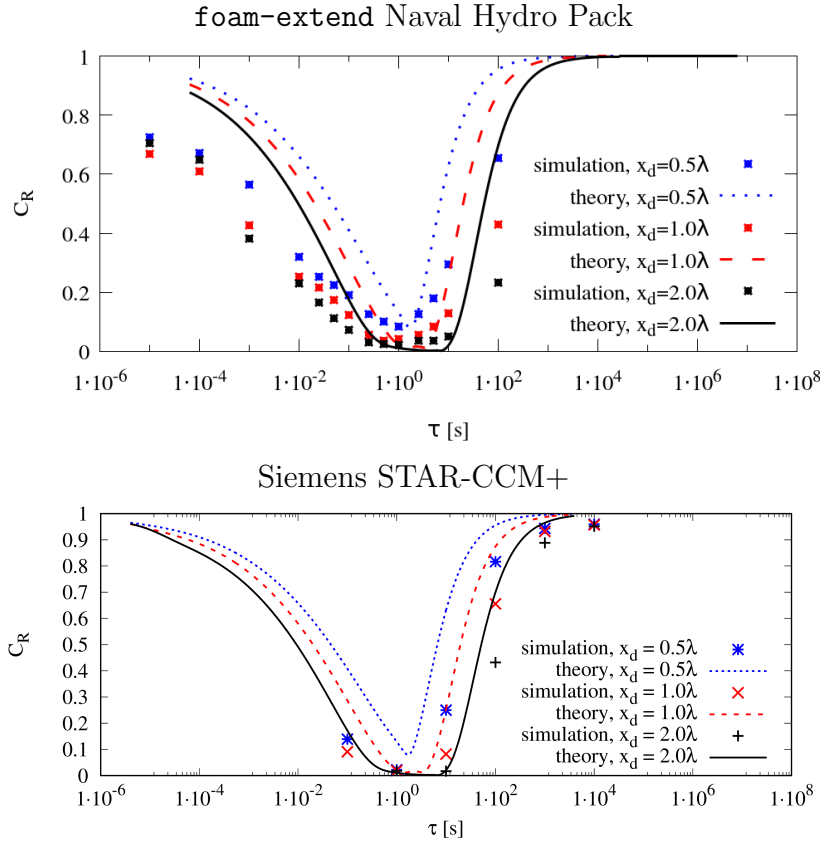


Figure 9: As Fig. 8, except that linear blending according to Eq. 7 with $n = 1$ was used

6.4. Relaxation towards background wave vs. relaxation towards calm water solution

In practice, the reference solution in relaxation zones is often the far-field wave. Thus the simulations from Sect. 6.1 were repeated with the reference solution set to the stream function solution for the far-field wave.

Figure 10 shows that, although Sects. 6.1 and 6.4 use substantially different reference solutions, again the optimum value for relaxation parameter τ is well predicted. Compared to Fig. 5 though, the values for C_R are much lower. Further, in Fig. 10 C_R is lower for the finer discretization than for the coarser discretization. This was expected, since the closer the solution within the simulation domain is to the reference solution, the smaller will the reflections become, since if $(u_{i,\text{ref}} - u_i) \rightarrow 0$ and $(\alpha_{i,\text{ref}} - \alpha_i) \rightarrow 0$ also $q_i \rightarrow 0$

and $q_\alpha \rightarrow 0$.

However, in practice the wave entering the relaxation zone usually does not correspond to the far-field wave, because it will be modified by wave reflecting bodies or discretization and iteration errors within the domain. Thus for the general case of forcing towards the far-field wave, one should rather expect reflection coefficients as in Fig. 6.

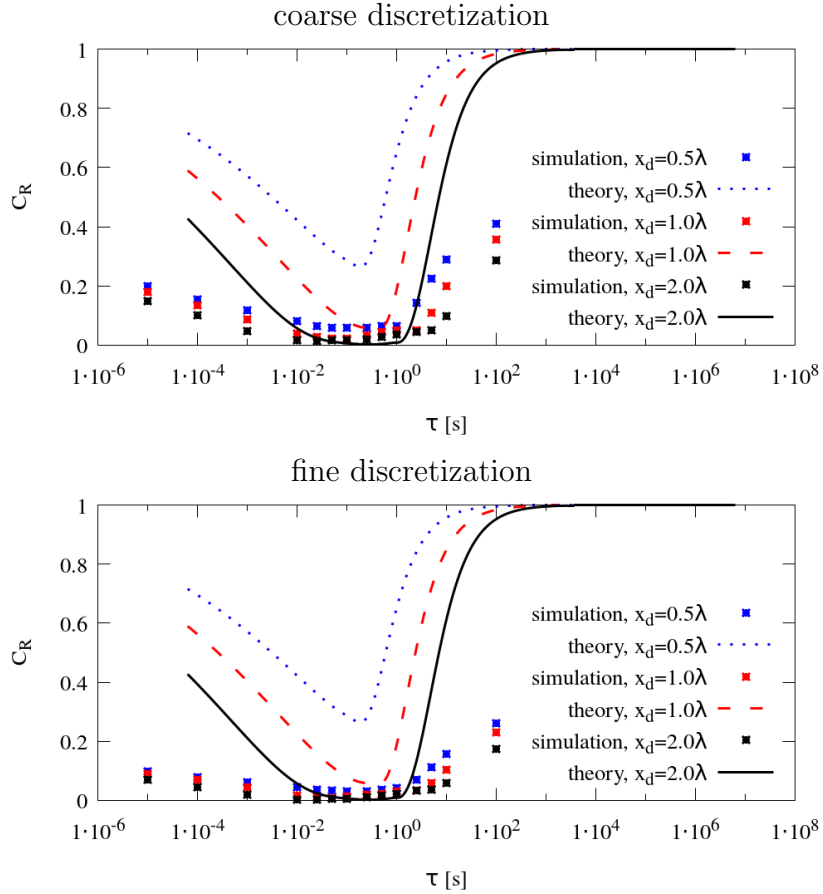


Figure 10: As Fig. 5, except for relaxation towards the far-field wave

6.5. Influence of choice of blending function

The simulations from Sect. 6.1 were repeated using different blending functions. Figure 11 shows results for power blending according to Eq. (7) for different relaxation parameter τ , different zone thickness x_d , and different

coefficients n . The results show good agreement between simulation and theory, indicating that the theory is a suitable tool for tuning the relaxation zone parameters.

One unexplained but perhaps not unwelcome feature in the simulation results occurs for large values of relaxation parameter τ . For $\tau \rightarrow \infty$ the relaxation source terms vanish to zero, so one would expect that the solution behaves as if there were no relaxation zone; this would result in a standing wave (i.e. $C_R \approx 1$), since the outlet boundary is nearly perfectly reflecting. Instead, the reflection coefficients remained significantly lower than 1, which becomes more pronounced for smaller values of n . It is possible that this is due to the term $(1 - b(\tilde{x}))$ on the left hand side of the governing equations, since if there is no reference solution to blend over to, then the blending out of the flow solution may behave like a damping. Note though that such large values of τ are not of practical interest since they cannot be used for combined generation and damping of waves as is illustrated in Sect. 7 in Figs. 14 and 15. Thus answering this question was considered outside the scope of this study and remains open for further research.

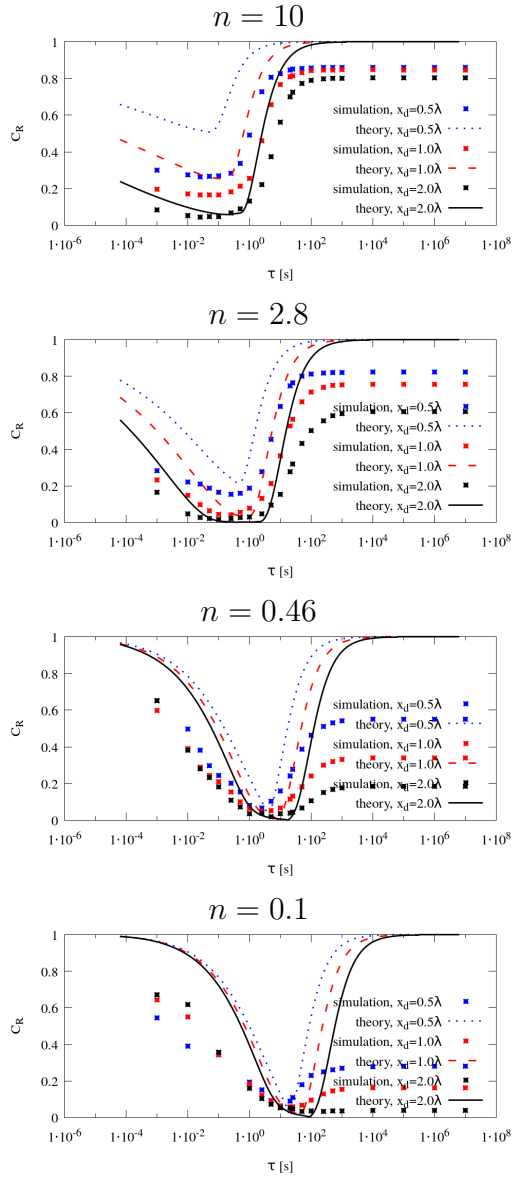


Figure 11: As Fig. 5, except for power blending with different values for exponent n ; theory predicts the shift in optimum value for τ when changing exponent n

Not only do the optimum values for τ and the shape of the curves for reflection coefficient C_R over τ change as seen in Fig. 11, but also the optimum choice of coefficient n depends on the zone thickness x_d as Figs. 12

and 13 demonstrate. For the investigated blending functions, the larger the relaxation zone thickness x_d becomes, the larger becomes the optimum value for n . For practical choices of x_d , the tendency seems to be that n should be > 1 for $x_d \gtrsim 1.5\lambda$, whereas for $x_d \lesssim 1.0\lambda$ then n should be < 1 .

Due to the complexity of the curves for $C_R(\tau)$, it is clear that no simple empirical relationship can be found for the optimum setting. Further, depending on the investigated wave spectrum a different tuning of the reflection-reducing characteristics of the relaxation zone may be appropriate. Thus it is recommended to use the theory to tune the forcing zone parameters to the wave of interest before each simulation. Note that the curves in this work are all for specific waves, and will shift sideways for waves of different periods.

It remains to say that by correctly tuning the relaxation zone parameters, the reduction of undesired wave reflections can be significantly improved, so that when correctly tuned already with a zone thickness of $0.5\lambda \leq x_d \leq 1.0\lambda$ (depending on the intended reflection coefficient) satisfactory results can be obtained, whereas with default settings an at least two to three times larger zone thickness would be required for the same reduction of undesired reflections.

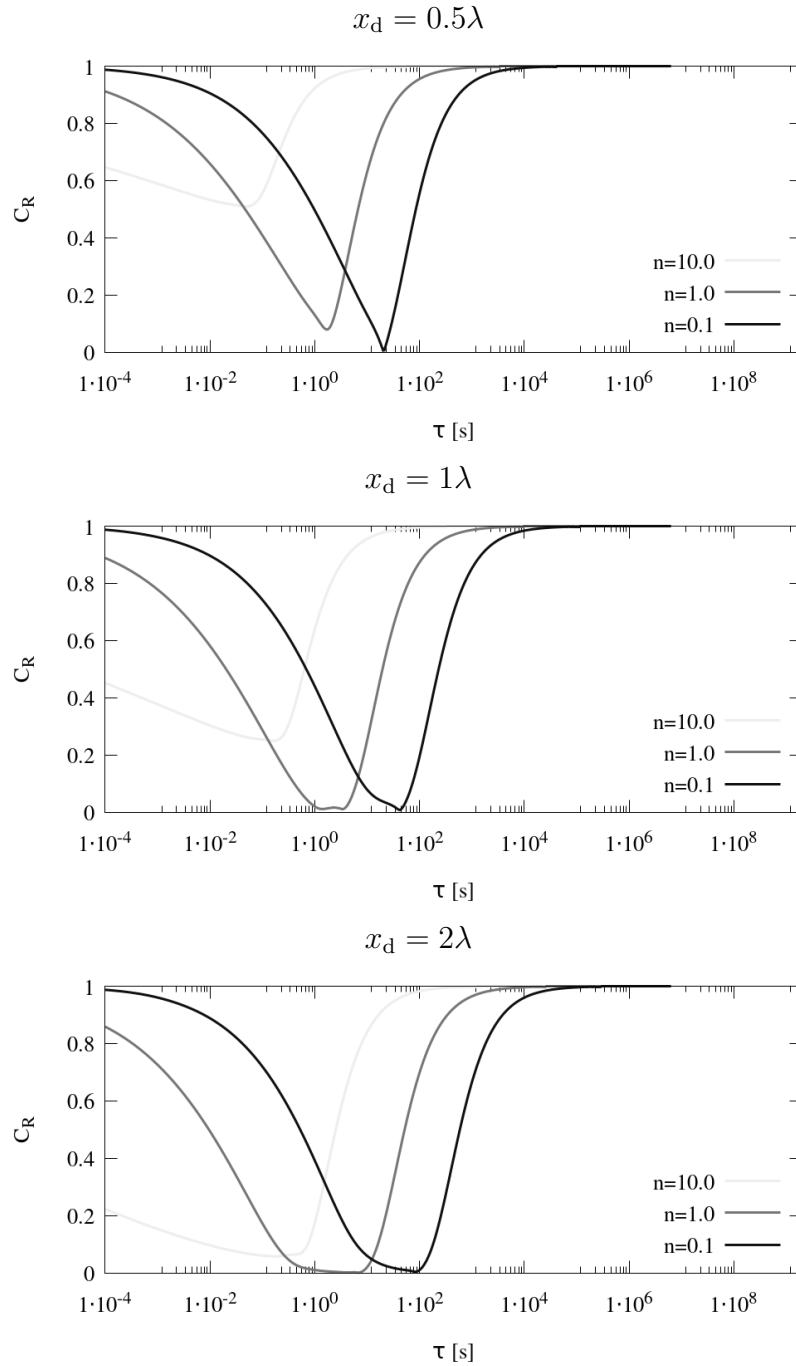


Figure 12: Theory predictions for reflection coefficient C_R over relaxation parameter τ for deep-water waves with period $T = 1.6$ s; for power blending according to Eq. (7) with different values for exponent n ;

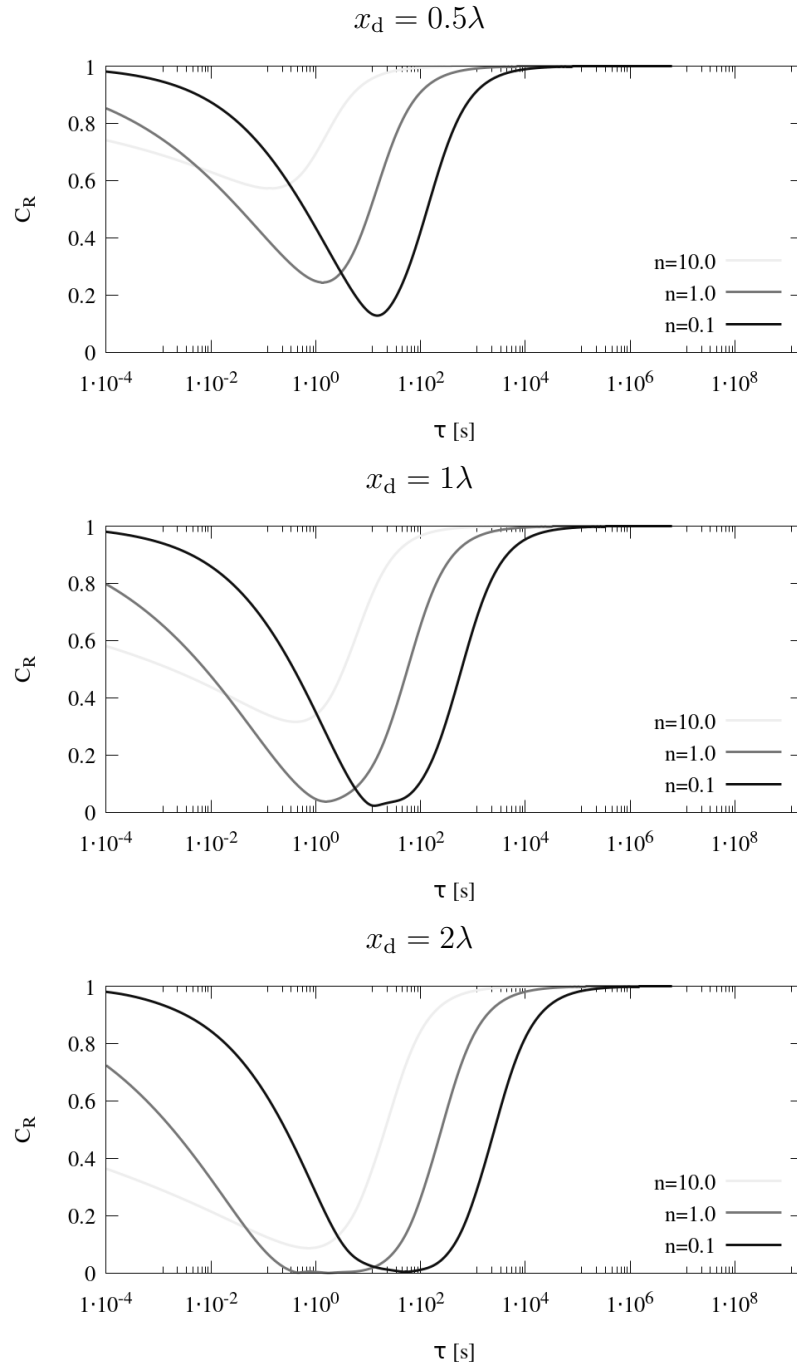


Figure 13: As Fig. 12, except for \cos^{2n} -blending according to Eq. (6) with different values for exponent n ; the optimum exponent n increases with increasing zone thickness x_d

7. Results of 3D-flow simulations

To investigate the validity of the present findings for practical 3D flow simulations, the flow around a strongly reflecting semi-submerged pontoon subjected to steep deep-water waves is simulated with the setup from Sect. 5. The solution domain was selected intentionally small, with relaxation zones attached to all vertical domain boundaries with a zone thickness of only $x_d \approx 0.7\lambda$. With respect to the tuning for the optimum blending function from Sect. 6.5, a power blending according to Eq. (7) with coefficient $n = 0.46$ was used. According to the theory prediction, a relaxation parameter of $\tau = 2.5$ s should provide a satisfactory reduction of undesired wave reflections ($C_R \approx 5\%$), while values larger or smaller by a factor of $10^{\pm 1}$ should produce significant reflections.

If reflections are satisfactorily reduced, then a periodic solution is expected to occur after several wave periods, and long-time simulations are possible without the accumulation of errors due to undesired wave reflections. Figure 14 shows that indeed such periodic results are obtained for the optimum setting. As shown in Fig. 15, too large values of τ damp not only undesired reflections but also the incident wave, while too small values produce wave reflections at the entrance to the relaxation zone, as can be also seen from the aperiodicity and change of amplitude of the forces on the pontoon.

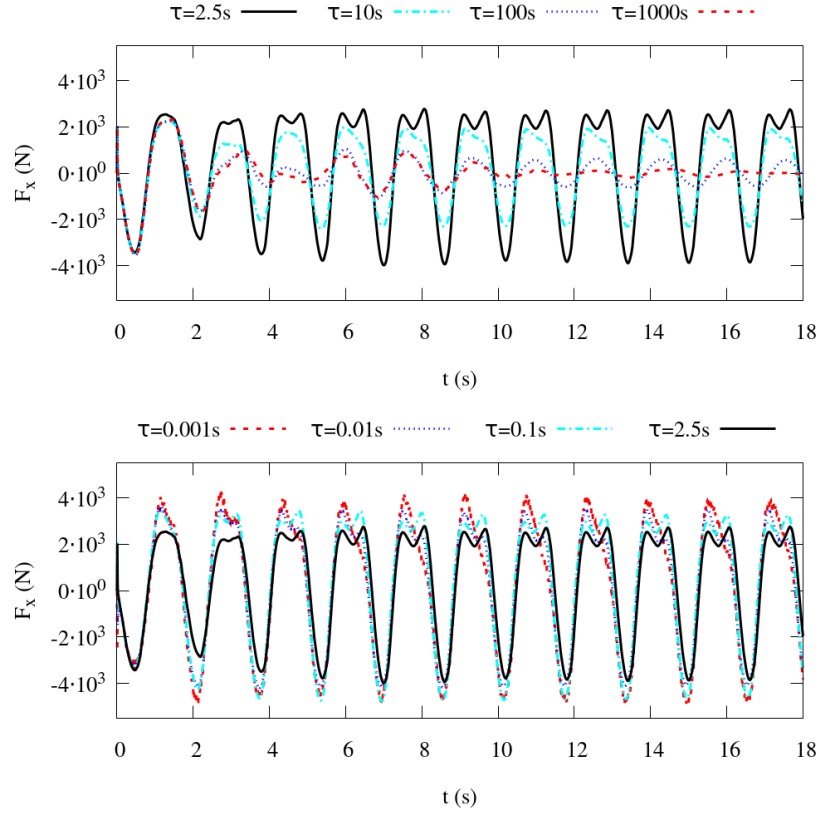
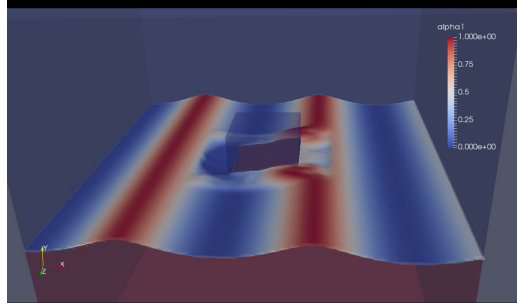
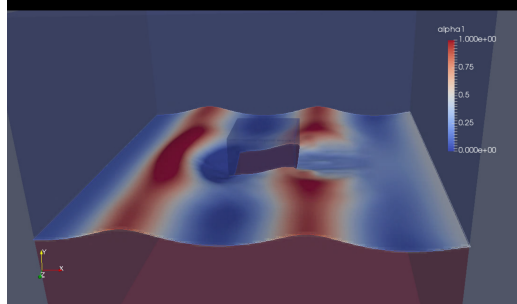


Figure 14: Force component in x -direction integrated over pontoon surface over time t for the *medium grid*; with relaxation zone thickness $x_d \approx 0.7\lambda$, power blending with exponent $n = 0.46$ and different values of relaxation parameter τ ; theory predicts an optimum of $\tau = 2.5\text{s}$, for which a periodic solution is obtained; the further τ deviates from the theoretical optimum, the stronger are the visible influences of undesired wave reflections in the results

too small relaxation parameter ($\tau = 0.01$ s)



\approx optimum relaxation parameter ($\tau = 2.5$ s)



too large relaxation parameter ($\tau = 100$ s)

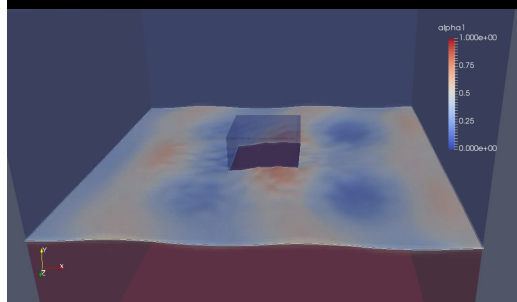


Figure 15: Simulation results for free-surface elevation at $t \approx 15$ s with too small ($\tau = 0.01$ s), too large ($\tau = 100$ s), and close-to-optimum ($\tau = 2.5$ s) choice of relaxation parameter τ ; for $\tau = 0.01$ s, the blending towards the far-field wave is too strong, so that reflection occurs mainly at the entrance to the relaxation zone; for $\tau = 100$ s, the blending towards the far-field is too weak, so that the far-field wave is not sustained; for $\tau = 2.5$ s, the waves reflected at the pontoon decay smoothly over the whole relaxation zone as intended

Figure 16 shows that the correct tuning of the relaxation zone enables a periodic solution for simulations over arbitrarily long simulation times.

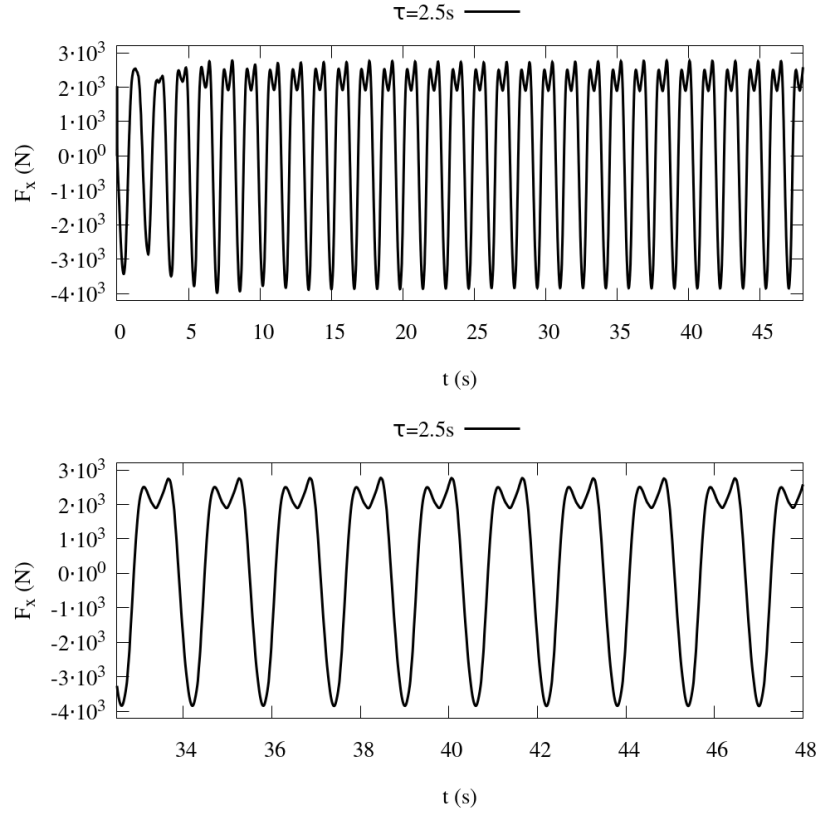


Figure 16: As Fig. 14, except for longer simulation duration; with close-to-optimum relaxation ($\tau = 2.5\text{s}$), simulations were run for $30T$ without noticeable accumulation of reflections

Figures 17 and 18 show that the difference between medium and fine grid is comparatively small, but for the coarse grid the force amplitudes are $\approx 10\%$ lower. For the present purposes all grids were considered suitable to demonstrate the benefits of tuning relaxation zones to the wave parameters.

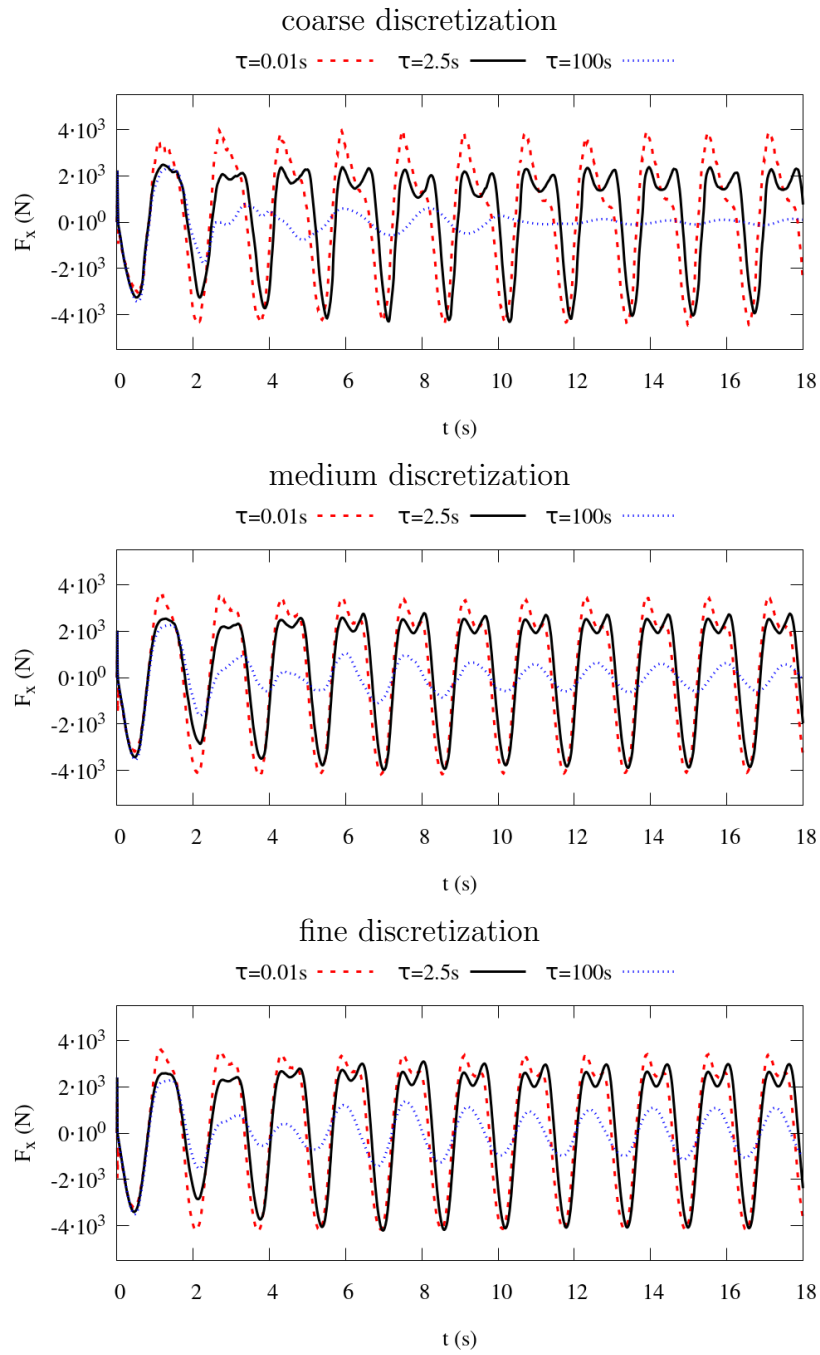


Figure 17: As Fig. 14, except for coarse, medium and fine discretization

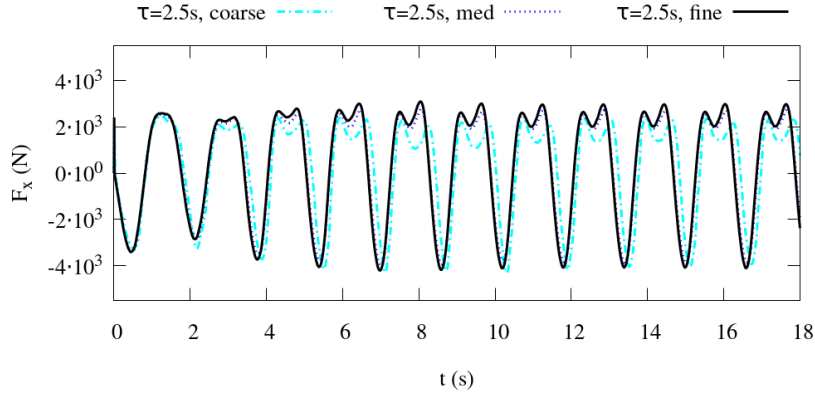


Figure 18: As Fig. 14, except for \approx optimum τ on coarse, medium and fine discretization; difference between the medium and fine discretization are small, so already medium discretization is considered acceptable

8. Conclusion

A theory was presented which predicts reflection coefficients for relaxation zones in flow simulations. It turned out to be a useful tool for tuning the case-dependent parameters of the relaxation zone *before running the flow simulations*. A simple computer program for evaluating the theory has been published as free software, which is expected to be applicable to all existing relaxation zone implementations.

The theory predictions were validated against flow simulation results using two different codes, the `foam-extend` Naval Hydro Pack and Siemens STAR-CCM+. Flow simulations of free-surface wave propagation with relaxation zones were run for shallow-water and deep-water conditions, different wave periods, wave steepnesses up to 71% of breaking steepness, different reference solutions and a wide range of settings for the case-dependent parameters of the relaxation zones. Theory predictions and simulation results showed satisfactory agreement.

Results showed that tuning the relaxation zone using the theory enables the use of significantly thinner zones and a reliable minimization of undesired wave reflections at the domain boundaries. Thus tuning relaxation zones using the present theory is recommended for engineering practice.

Acknowledgements

The study was supported by the Deutsche Forschungsgemeinschaft (DFG) with grant AB 112/11-1.

References

- [1] Chen, H. C., Yu, K., and Chen, S. Y., 2006. Simulation of Wave Runup Around Offshore Structures by a Chimera Domain Decomposition Approach. *Proc. Civil Engineering in the Oceans VI*, 267-280.
- [2] Carmigniani, R. A., Violeau, D. 2018. Optimal Sponge Layer for water waves numerical models. *Ocean Eng.*, 163.
- [3] Choi, J. and Yoon, S. B. 2009. Numerical simulations using momentum source wave-maker applied to RANS equation model, *Coastal Engineering*, 56 (10), 1043-1060.
- [4] Colonius, T., 2004. Modeling artificial boundary conditions for compressible flow. *Ann. Rev. Fluid Mech.*, 36, 315-345.
- [5] Ferziger, J., Perić, M., 2002. *Computational Methods for Fluid Dynamics*. Springer, Berlin.
- [6] Jacobsen, N. G., Fuhrman, D. R., Fredsøe, J. 2012. A wave generation toolbox for the open-source CFD library: OpenFoam®. *International Journal for Numerical Methods in Fluids*, 70 (9), 1073-1088.
- [7] Jasak, H., Vukčević, V., Gatin, I., 2015. Numerical Simulation of Wave Loads on Static Offshore Structures. in: *CFD for Wind and Tidal Offshore Turbines*, Springer Tracts in Mechanical Engineering, Cham, pp. 95-105. ISBN 978-3-319-16201-0, <http://dx.doi.org/10.1007/978-3-319-16202-7>.
- [8] Kim, J., O’Sullivan, J., Read, A. 2012. Ringing analysis of a vertical cylinder by Euler overlay method. *Proc. OMAE2012*, Rio de Janeiro, Brazil.
- [9] Mani, A., 2012. Analysis and optimization of numerical sponge layers as a nonreflective boundary treatment. *J. Comput. Phys.*, 231 (2), 704-716.

- [10] Mayer, S., Garapon, A., Sørensen, L., 1998. A fractional step method for unsteady free-surface flow with applications to non-linear wave dynamics. *Int. J. for Num. Meth. in Fluids*, 28 (2), 293-315.
- [11] Meyer, J., Graf, K., Slavic, T. 2017. A new adjustment-free damping method for free-surface waves in numerical simulations. *In: ICNME. VII Intl. Conf. Computational Methods in Marine Engineering MARINE 2017*, Nantes, France.
- [12] Park, J. C., Kim, M. H., Miyata, H., 1999. Fully non-linear free-surface simulations by a 3D viscous numerical wave tank, *Int. J. Numerical Methods in Fluids*, Vol. 29, No. 6, 685-703.
- [13] Park, J. C., Kim, M. H., Miyata, H., 2001. Three-dimensional numerical wave tank simulations on fully nonlinear wave-current-body interactions. *Journal of Marine Science and Technology*, 6 (2), 70-82.
- [14] Perić, R., Abdel-Maksoud, M., 2016. Reliable damping of free-surface waves in numerical simulations. *Ship Technology Research*, 63 (1), 1-13.
- [15] Perić, R., Abdel-Maksoud, M., 2018. Analytical prediction of reflection coefficients for wave absorbing layers in flow simulations of regular free-surface waves. *Ocean Engineering*, 147, 132-147.
- [16] Rienecker, M.M., Fenton, J.D., 1981. A Fourier approximation method for steady water waves. *Journal of Fluid Mechanics*, 104, 119-137.
- [17] Schmitt, P., and Elsaesser, B., 2015. A review of wave makers for 3D numerical simulations. *Marine 2015*, 6th Int. Conf. on Computat. Methods in Marine Eng., Rome, Italy.
- [18] Ursell, F., Dean, R. G., Yu, Y. S., 1960. Forced small-amplitude water waves: a comparison of theory and experiment. *J. Fluid Mech.*, 7 (01), 33-52.
- [19] Vukčević, V., Jasak, H., Malenica, Š. 2016a. Decomposition model for naval hydrodynamic applications, Part I: Computational method. *Ocean Engineering*, 121, 37-46.
- [20] Vukčević, V., Jasak, H., Malenica, Š. 2016b. Decomposition model for naval hydrodynamic applications, Part II: Verification and validation. *Ocean engineering*, 121, 76-88.

- [21] Weller, H.G., Tabor, G., Jasak, H., Fureby, C., 1998. A tensorial approach to computational continuum mechanics using object oriented techniques. *Comput. Phys.* 12, 620-631.
- [22] Wöckner-Kluwe, K., 2013. Evaluation of the unsteady propeller performance behind ships in waves. *PhD thesis at Hamburg University of Technology (TUHH)*, Schriftenreihe Schiffbau, 667, Hamburg.